Received: 20 March 2023 | Revised: 3 June 2023 | Accepted: 8 June 2023

DOI: 10.1002/app.54405

RESEARCH ARTICLE

Journal of Applied Polymer Science WILEY

High-consistency silicone rubber with reduced Young's modulus. An industrial option to dielectric silicone rubber

Joaquim Mª Rius-Bartra[1,2] | **Norma Ferrer-Serrano**[1] | **Núria Agulló**[2] | **Salvador Borrós**[2]

[1]R&D Department, Venair Ibérica SAU, Terrassa, Spain

[2]Grup d'Enginyeria de Materials (GEMAT), Institut Químic de Sarrià (IQS), Universitat Ramon Llull, Barcelona, Spain

Correspondence
Salvador Borrós, Grup d'Enginyeria de Materials (GEMAT), Institut Químic de Sarrià (IQS), Universitat Ramon Llull, Barcelona 08017, Spain.
Email: salvador.borros@iqs.url.edu

Funding information
AGAUR, Grant/Award Numbers: 2018-DI062, SGR 2021

Abstract

Flexible capacitive sensors based on silicone rubber have gained importance in both academic and industrial fields due to their advantages, including low power consumption and high stability to temperature, and humidity. However, pristine silicone rubber has a low dielectric constant (ε'), requiring the use of dielectric additives such as TiO_2, $BaTiO_3$, or Sb_2O_3-doped SnO_2 rutile-modified particles (ATO) to enhance electrical properties, but they also increase Young's modulus (E). To overcome this problem, liquid silicone rubbers (LSR) are commonly used in academic research due to their low E, but they often compromise mechanical integrity. In contrast, high-consistency silicone rubbers (HCR), the industry commodity, maintain mechanical integrity even at high filler loadings but are limited in their use in dielectrics due to high E values. This paper explores the potential of vinyl-terminated HCR for developing dielectric composites with high electromechanical response, with an improved ε' and a reduced E while retaining mechanical and processability properties. The resulting dielectric HCR formulations exhibit optimal properties for developing flexible capacitive sensors using well-established industrial products and processes.

KEYWORDS

capacitive sensors, dielectric constant, electroactive polymers, flexible sensors, high-consistency silicone rubbers, liquid silicone rubbers, transductors

1 | INTRODUCTION

In recent years, the integration of flexible sensors has become a relevant field in the industry, keeping up with the constant emergence of new technologies, such as movement, positioning, and force sensing in robotics and mobile equipment, structural monitoring of industrial equipment and transport vehicles and health and biosensors.[1–3] As a result, the research in new polymeric and elastomeric materials has focused on the design of innovative sensors.[4–9]

Capacitive sensors are of interest due to their low power consumption, high accuracy, and stability to temperature and humidity.[10,11] The use of polymeric materials is the main strategy to produce flexible capacitive sensors, where thermoplastics are the most used in the research. Examples include polyethylene, polyimide, or polyethylene terephthalate. Among these materials, silicone rubber stands out with its exceptional elastomeric properties. They present higher flexibility and elasticity, allowing the silicone rubber to be easily stretched, bent, or

compressed. The low hysteresis upon deformation allows the repeated deformation of silicone rubber, which is essential for the durability of the sensors. Silicone rubber exhibits high thermal resistance for high-temperature applications, with typical operating temperatures ranging from 200 to 300°C. Their excellent electrical insulation and dielectric strength ensure safe use in electrical applications and facilitate the enhancement of dielectric constant while the electrical insulation capacity is retained.

However, pristine silicone rubber has a low dielectric constant, typically between 2.7 and 3.0, which depends on the silica loading. To improve its electrical properties, this type of material must be modified using dielectric additives. Although there are many strategies available to enhance silicone rubber's electrical properties, achieving balanced electromechanical and processability properties remains challenging.[12–14] This represents additional drawbacks in their transference to the industry field, which requires more specific strategies that prioritize the use of commercial products and standard industrial procedures.

The equation of Maxwell pressure (p_M) is commonly used to describe the electromechanical response of capacitive sensors when low strains are applied. This equation shows the relationship between the capacitance of the sensor and the mechanical response:

$$s = \frac{p_M}{E} = \frac{\varepsilon_0 \varepsilon'}{E}\left(\frac{U}{d}\right)^2, \quad (1)$$

where s is the strain, U is the voltage applied, d is the thickness of the dielectric composite, ε_0 is the permittivity at vacuum, ε' is the dielectric constant, and E is Young's modulus. To improve the electromechanical response of the sensor, the ratio $\varepsilon_0 \varepsilon' E^{-1}$ must be maximized, but both properties are related thru the effect of the dielectric additive to both electrical and mechanical properties, which will have a significant impact on the overall performance of the composite. From the point of view of sensor application, increasing the dielectric constant value of the composite will enhance the device's capacitance, and thus, the sensitivity of the sensor. On the other hand, the reduction of Young's modulus will make a softer material, easier to be deformed, and thus, the sensibility of the sensors can be enhanced. Unfortunately, the improvement of the dielectric constant, Young's modulus, mechanical integrity, or processability is often at the expense of the other parameters.

One of the most usual strategies to improve dielectric constant is the blend of metal oxides or ceramic fillers, such as TiO_2 or $BaTiO_3$, with a silicone rubber matrix.[15–20] Significant challenges arise when using these dielectric fillers in capacitive sensors, as these materials often require high loading concentrations to substantially increase the dielectric constant. This is mainly due to the relatively low dielectric constant in comparison to conductive materials and the difficulties in achieving proper dispersion or chemical compatibility with the matrix. However, these materials allow the retention of the electrical insulation behavior of the matrix, while dielectric loss is not significantly modified, which is the main advantage over the use of conductive particles. An alternative approach that has garnered attention is the utilization of core-shell particles in the field of sensors. Core-shell particles exhibit a unique characteristic where the properties of the materials used in the core and shell interact synergistically, resulting in enhanced performance that cannot be achieved by either substance alone. In this case, combining a dielectric oxide with a conductive material within the core-shell structure is expected to generate a synergistic effect, leading to improved dielectric constant while retaining the electrical insulation capacity and minimizing dielectric loss. In addition, the controlled morphology of these particles is also expected to facilitate their dispersions, improving the overall properties of the dielectric silicone rubber.[21–25]

In this study, we propose the industrially available Sb_2O_3-doped SnO_2 rutile-modified particles, also known as TiO_2/SnO_2-Sb core-shell particles (ATO).[26,27] The conductive layer and TiO_2 core are polarizable within an electrical field, so it is expected that this filler will greatly enhance the effective dielectric constant of their composites compared to TiO_2 and $BaTiO_3$. While ATO particles have not been extensively explored for this specific purpose previously, they have found widespread application in the fabrication of gas sensors, showcasing their potential for functional material design and integration.[28–30]

The addition of large quantities of dielectric fillers increases Young's modulus, depending on the type of particle used. This often leads to modest improvement in the dielectric constant but significant hardening of the composite, resulting in overall poor performance.[13,14] Consequently, the selection of the silicone rubber matrix and its processing play a crucial role in developing a dielectric silicone with a balanced combination of dielectric constant, Young's modulus, and mechanical integrity. Silicone rubber can be classified into two main groups: high-consistency silicone rubber (HCR) and liquid silicone rubber (LSR), which determine the processing capacity of the formulations and the mechanical properties of the dielectric composite.

HCR is the most used type of silicone rubber in the industrial sector. It is processed using internal mixers and two-roll mills, which are standard methods in the rubber industry. The viscosity increase caused by fillers is not a major concern during the processing of HCRs due to the high shear provided by industrial equipment. These rubbers are formulated to have a high Young's modulus, making them suitable for use as elastic

materials. This is achieved by using silicone gum with a high vinyl group content and adding silica to improve its mechanical properties.[31–34] The processing of highly filled HCR is a well-established practice in the industry, facilitating the dispersion of dielectric fillers and the production of composites with high dielectric constants.[35,36] Although HCRs are widely used, their high Young's modulus of standard grades makes them unsuitable for use as dielectric silicone in flexible sensors that require a lower modulus. Therefore, HCR matrices must be formulated specifically, taking advantage of the availability of diverse types of HCR gums in the market, to overcome this problem.

To address this issue, academic research has focused on using LSR as the matrix in dielectric silicone rubber composites. LSRs offer advantages such as an initially low Young's modulus and easy processability in laboratory equipment due to their liquid-like consistency.[37–40] In LSR formulations, the location and quantity of vinyl groups within the silicone chains are often manipulated to regulate the crosslinked structure and enhance rubber flexibility. For example, low molecular weight vinyl-terminated silicone fluids can be utilized.[37,38] Extrapolating this strategy to HCR, it could potentially be applied by using commercially available vinyl-terminated silicone gums. By modifying the network structure, it is possible to tailor the final mechanical properties of the material according to specific requirements, as observed in LSR composites.

The aim is to achieve high dielectric filler loading while retaining Young's modulus, resulting in a composite that can be processed with the standard industrial procedure and well-balanced electromechanical properties to be used in flexible sensors. The ideal composite should have a low Young's modulus (E) of less than 1 MPa and a high dielectric constant (ε') greater than five while having sufficient mechanical integrity and processing capabilities. This study will assess the effect of the silicone matrix and filler types on the electromechanical properties of the composites. The vinyl-terminated HCR matrix (ViT) formulated for this study will be compared to an electrical-grade LSR (55P) and a standard-grade HCR (USP). Furthermore, as a potential dielectric filler, ATO particles will be compared to TiO_2 and $BaTiO_3$. The evaluation will focus on substantially improving the dielectric constant while maintaining mechanical properties.

2 | EXPERIMENTAL SECTION

2.1 | Materials

Rutile particles from DuPont (Ti-Pure™ R-902+, 0.4 μm, 4.0 g cm^{-3}, $\varepsilon' = 100$), $BaTiO_3$ from Acros Organics (99%, 1.052 μm, 6.08 g cm^{-3}, $\varepsilon' = 1700$), core-shell particles TiO_2@SnO_2-Sb from Milliken Chemical BE (Zelec 1410 T, 1 μm, 4.47 g cm^{-3}), two-parts addition cured electrical-grade LSR from Dow (Silastic™ HV 1551-55P, 1.09 g cm^{-3}, ε'=2.8), standard transparent USP VI/FDA grade 50 ShA HCR (1.14 g cm^{-3}), ([Vi] = 102 ppm, Mw = 581,264 g mol^{-1}, 0.97 g cm^{-3}, $\varepsilon' = 2.72$), hydrophobic fumed silica (BET = 240 m^2 g^{-1}, 2.11 g cm^{-3}, $\varepsilon' = 3.8$), commercial two-parts addition curing system for HCR.

2.2 | Composites preparation

LSR composites were prepared with Speedmixer DAC 400. FVZ from Hauschild Engineering. First, the dielectric filler was pre-dispersed in each part of the LSR kit in 10 steps of 30 s at 2750 rpm, followed by 5 min of refrigeration at −10°C. Then the two parts are mixed at a 1:1 ratio, as per manufacturer indications, for more than 4 steps. It must be pointed out that ATO interferes in the curing reaction, and since the matrix structure is crucial for characterization, this filler will not be used in the LSR matrix. However further studies will be done.

Vinyl-terminated silicone rubber composites were prepared in an AME-7 (322 kW) internal mixer (322 kW) from Lleal, S.A where silicone gum and fillers were added. The curing system for HCR composites was added in a two-roll mill by first adding Part B which held the inhibitor and crosslinker, followed by Part A with Karstedt's catalyst. The curing system was added following the manufacturer's recommendations. The specific gravity of the ViT matrix is 1.0969 ± 0.0007 g cm^{-1}.

All samples were cured at 150°C for 10 min in a laboratory press at 240 bar from Gibitre Instruments SRL (ISO 23529)[41] and post-cured at 180°C for 2 h in an air-recirculating oven UT 6420 from Thermo Scientific GmbH. The stress–strain samples were prepared in a 20 × 20 × 0.2 cm mold and dielectric films were prepared within two smooth molds. The molds used are hard chrome-plated steel. The silicone rubber composites have been named according to Table 1.

2.3 | Characterization

Stress–strain and tear strength were evaluated in a Zwick/Roell Z005 (ISO 34-method B and ISO 37-type 1).[42,43] The modulus at different deformation have been automatically determined following ISO 37. The chord slope between the modulus at 25% and 10% of strain has been used for the determination of Young's modulus.

Impedance was analyzed with Autolab PGSTAT302N with FRA32M module at 0 V (open-circuit potential)

TABLE 1 Nomenclature and formulations of the silicone composites prepared.

Silicone rubber matrix	Sample	Dielectric filler (phr)		
		TiO_2	$BaTiO_3$	ATO
LSR SilasticTM HV-1551-55P (55P)	55P			
	55P_T50	50		
	55P_T100	100		
	55P_B50		50	
	55P_B100		100	
Vinyl-terminated HCR (ViT)	ViT			
	ViT_T50	50		
	ViT_T100	100		
	ViT_B50		50	
	ViT_B100		100	
	ViT_A50			50
	ViT_A100			100
Standard-grade HCR (USP)	USP			
	USP_T100	100		
	USP_B100		100	
	USP_A100			100

equipped with a custom sample holder with Ø50 mm guarded stainless steel 316 electrodes. A torque force of 2.0 ± 0.2% N·m was applied with a digital dynamometer from Fervi SpA. All impedance measurements were performed inside a Faraday cage. The design was initially based on Müller et al.[44] in which the sample holder was re-designed to uniformly apply pressure to the sample and to meet the measure standard requirements (ASTM D150).[45–48]

3 | RESULTS AND DISCUSSION

3.1 | Electrical insulation characterization

The primary factor in determining if a composite can be used as a dielectric material is its electrical insulation capacity, otherwise, this material is considered a piezoresistive material, and its application fall within other technologies. The limit for insulating materials is typically considered to be 10^{-8} S cm^{-1}. Ideally, the composite should have the lowest value possible to minimize the risk of premature electrical failure. Using the impedance analysis of the composites, it is possible to obtain the electrical conductivity as a function of the frequency. In the low-frequency range, a plateau is typically observed, which is related to direct current (DC) conductivity. The impedance method is effective in evaluating the insulation performance of composites using low-voltage analysis.[49,50] The conductivity results are presented in Figure 1.

The conductivity of the 55P composites does not show a significant change with the addition of the dielectric fillers. The same trend is also seen in ViT composites with ATO and $BaTiO_3$ at 50 phr, but not with TiO_2, which increases the conductivity by two orders of magnitude. At 100 phr, the conductivity at 1 Hz increases by two orders of magnitude for all fillers. Furthermore, the ATO composites exhibit a steeper slope compared to TiO_2 and $BaTiO_3$, which is attributed to the presence of confined charges in the conductive layer that can interact with the electric field at higher frequencies. All the composites studied have conductivities at 1 Hz below 10^{-12} S cm^{-1}, indicating that they are insulators.

To determine if the composites are suitable to be used in capacitive devices, the dielectric loss must be also characterized. This parameter, usually expressed as loss tangent ($\tan\delta$), describes the effect of the dielectric relaxation and conductive processes that dissipate electric field energy into heat and should be as lower as possible.[13] The results of the $\tan\delta$ are presented in Figure 2.

TiO_2 and $BaTiO_3$ exhibit dielectric relaxation in the frequency range below 100 Hz, where the dielectric loss decreases with a significant slope up to 10 Hz, which is associated with the interfacial polarization of charges within the particles and increases with the concentration of the dielectric filler.[20,51–53] However, the composite with 50 phr of ATO does not show significant relaxation

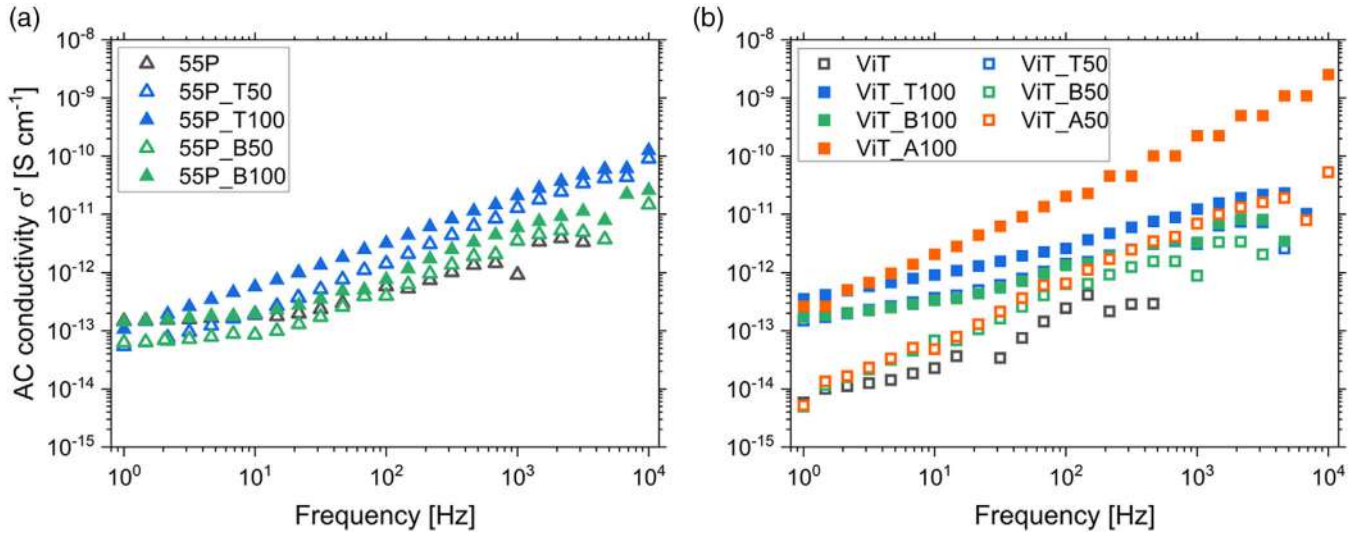

FIGURE 1 AC conductivity (S cm^{-1}) of (a) 55P and (b) ViT composites. [Color figure can be viewed at wileyonlinelibrary.com]

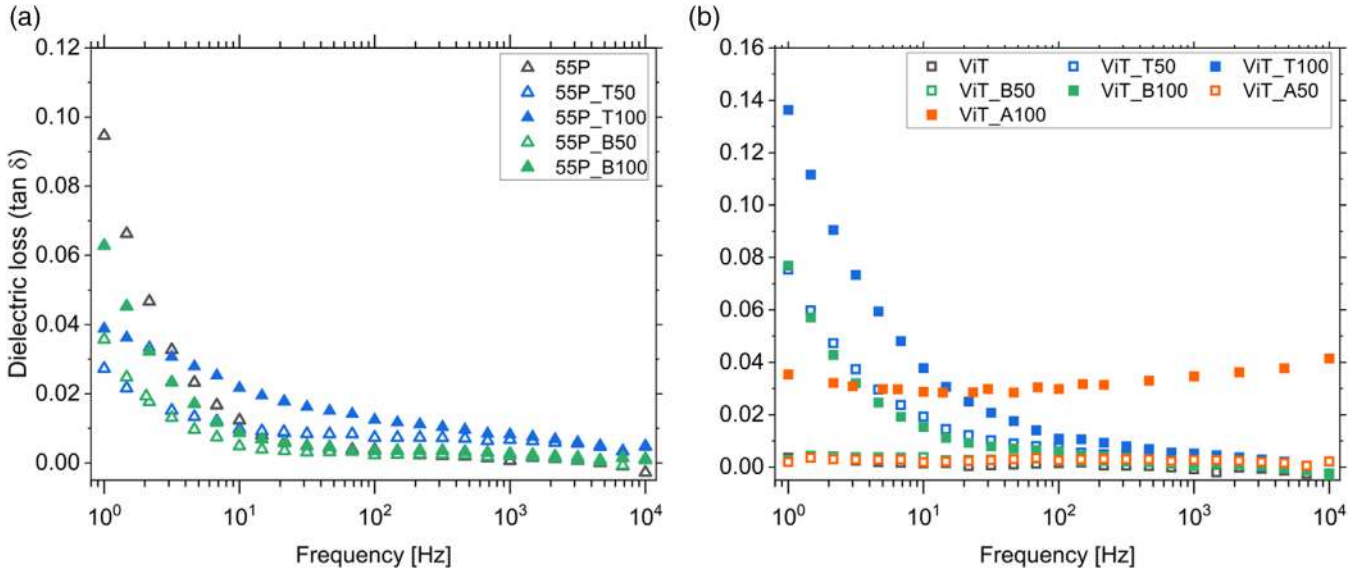

FIGURE 2 Dependency on the frequency of tan δ for (a) matrix and 50 phr and (b) 100 phr composites. [Color figure can be viewed at wileyonlinelibrary.com]

in the studied frequency range. With 100 phr loading, a slightly positive slope is observed above 100 Hz, likely due to increased space-charge polarization. This trend is dependent on the filler concentration and is characterized by a high relaxation time caused by charges accumulated at the aggregate boundaries, which cannot follow the alternating field.[54–58]

3.2 | Dielectric constant characterization

The dielectric constant as a function of frequency is shown in Figure 3. The results reveal that there is a slight difference between the matrices, suggesting that the dielectric constant is primarily a result of filler concentrations. Thus, the network structure modification when using vinyl-terminated HCR does not affect the dielectric response. The addition of 50 phr TiO_2 and $BaTiO_3$ slightly increases the dielectric constant, but there is no significant difference observed between them. At a concentration of 100 phr, TiO_2 shows higher values than $BaTiO_3$. However, the composite barely meets the desired dielectric constant value of $\varepsilon' = 5$. Conversely, ATO particles have a pronounced effect on the enhancement of the dielectric constant. The composite ViT_A50 with 50 phr ATO particles have a dielectric constant of

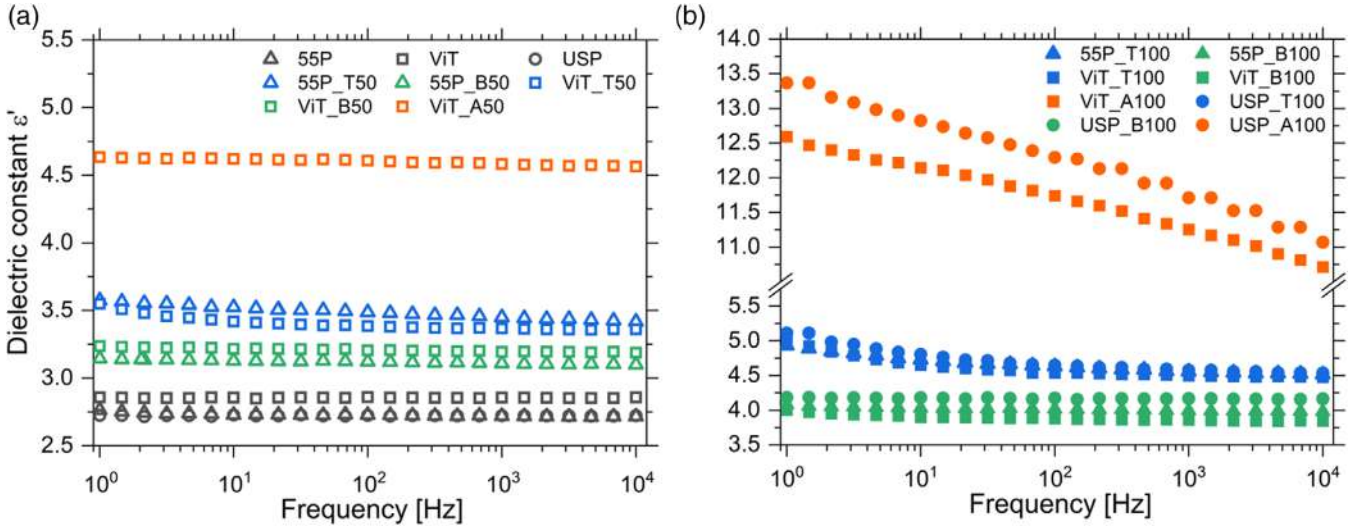

FIGURE 3 Dependency on the frequency of dielectric constant for (a) matrix and 50 phr and (b) 100 phr composites. [Color figure can be viewed at wileyonlinelibrary.com]

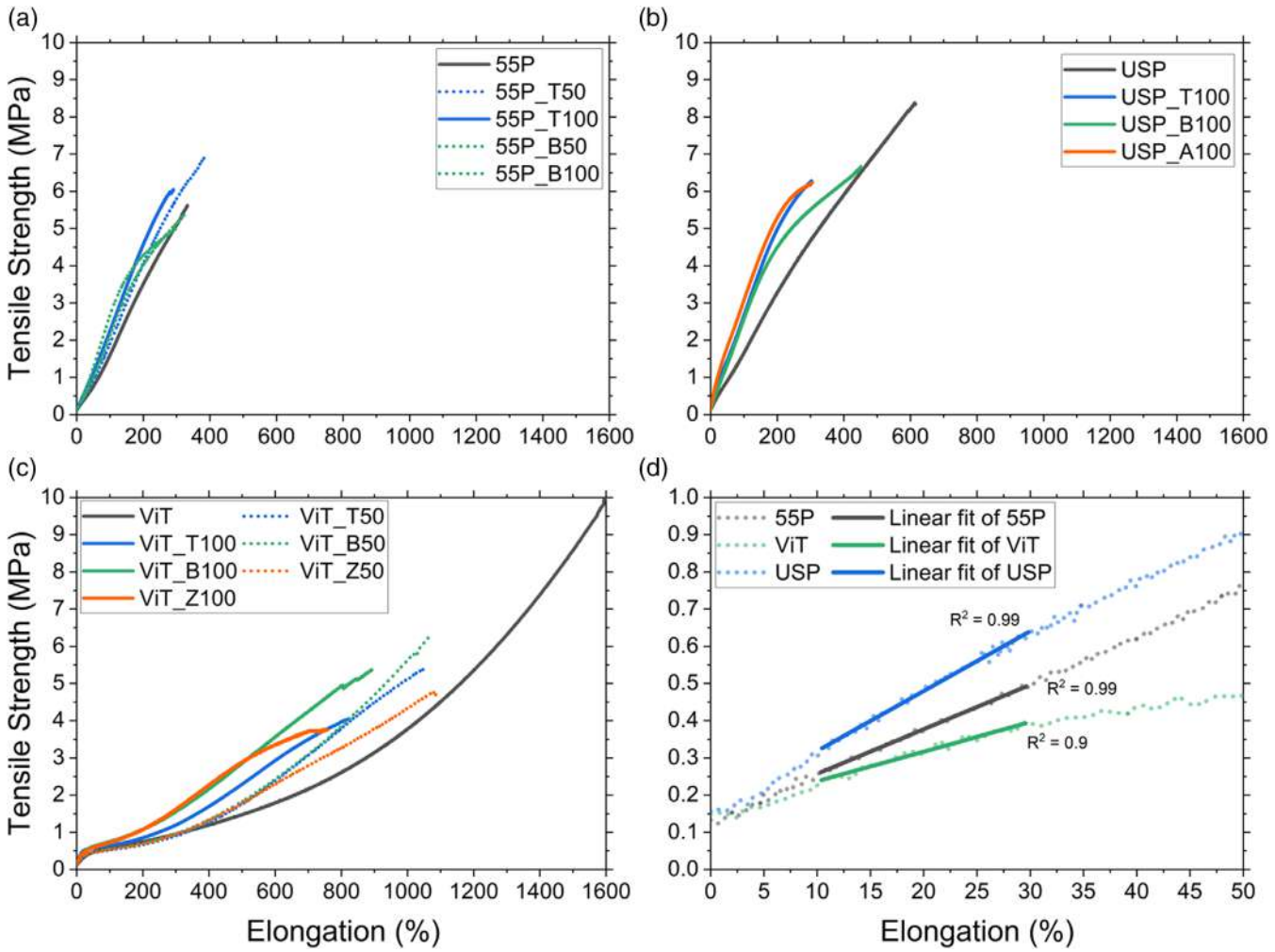

FIGURE 4 Mean stress–strain curves of composites of (a) LSR matrix, (b) standard-grade HCR, (c) vinyl-terminated HCR, and (d) example of linear fit with silicone matrices. [Color figure can be viewed at wileyonlinelibrary.com]

TABLE 2 Young's modulus (MPa) for the different composites.

Young's modulus [MPa]	55P	ViT	USP
Matrix	1.23 ± 0.03	0.85 ± 0.03	1.7 ± 0.1
T50	1.56 ± 0.05	0.82 ± 0.09	
T100	1.9 ± 0.2	0.96 ± 0.04	2.6 ± 0.2
B50	1.57 ± 0.04	0.86 ± 0.04	
B100	2.06 ± 0.07	1.19 ± 0.09	2.5 ± 0.1
A50		0.71 ± 0.06	
A100		1.06 ± 0.09	3.4 ± 0.2

$\varepsilon' = 4.6 \pm 0.2$ at 100 Hz, comparable to the values of TiO_2 and $BaTiO_3$ at 100 phr. At a concentration of 100 phr, the dielectric constant reaches large values of $\varepsilon' = 11.9 \pm 0.7$ at 100 Hz.

The dielectric constant of TiO_2 and $BaTiO_3$ composites follows the same trend as the $\tan\delta$, with the apparent higher dielectric constant at low frequencies attributed to interfacial polarization. For composites containing ATO particles, a dependency across the entire frequency range studied is only observed at a loading of 100 phr, which confirms the presence of space-charge polarization, as indicated by the $\tan\delta$ analysis.

3.3 | Mechanical properties

The stress–strain behavior of the composites is shown in Figure 4 and the corresponding Young's modulus values are presented in Table 2. The Young's modulus has been determined by the chord slope between 10% and 25% of deformations by the equation

$$E = \frac{\sigma_{25\%} - \sigma_{10\%}}{\varepsilon_{25\%} - \sigma_{25\%}}, \quad (2)$$

where E is the chord Young's modulus, σ_i is the tensile at given deformation, and ε_i is the stress. This region has presented a particularly linear behavior within all the samples prepared, allowing the comparison between the different matrices, as can be seen in Figure 4c.

The 55P and USP matrices exhibit the same elastic response that is typical of general-purpose silicone rubbers. This is due to the random distribution of vinyl groups along the polymer chains responsible for the final network obtained. The ViT matrix, on the other hand, has crosslinking joints only at the ends of the silicone chains, resulting in a higher degree of freedom with increased flexibility. The difference in the crosslinking distribution can be observed with the higher Young's modulus of the LSR and USP matrices, while ViT has a significantly lower modulus.

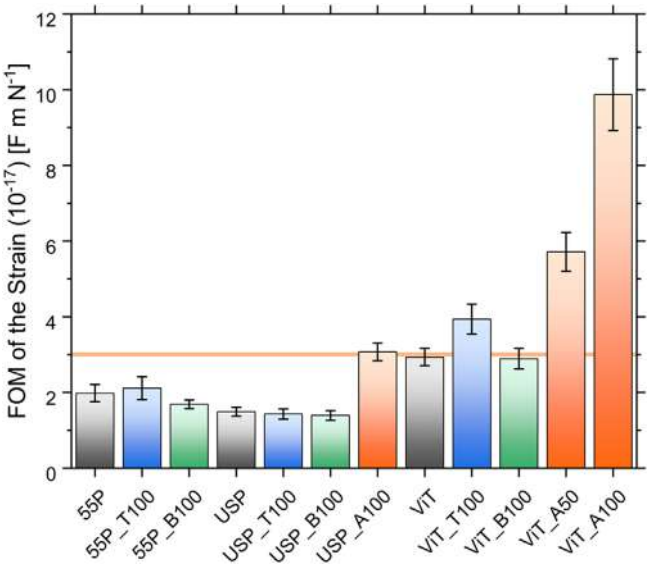

FIGURE 5 The figure of merit of strain for the dielectric silicone composites and objective line. [Color figure can be viewed at wileyonlinelibrary.com]

The results show that the addition of TiO_2 to the 55P matrix increases both the ultimate tensile strength and elongation, as well as Young's modulus due to the filler's reinforcing effect. On the other hand, the addition of $BaTiO_3$ results in slight decreases in the ultimate properties while Young's modulus still increases similarly to when TiO_2 is added. The results in USP composites show a similar trend in the increase of Young's modulus but with a significant reduction in the ultimate properties. The formulations with ViT retain the matrix's flexibility and relatively high levels of elongation even with higher loads of filler.

3.4 | FOM for silicone sensors

Since the function of the material as a sense requires a combination of properties to achieve good operating properties, the overall performance of the sensor will be assessed using a Figure of Merit (FOM_{strain}),[59] which relates the dielectric constant and Young's modulus, as defined in Equation (2):

$$FOM_{strain} = \frac{\varepsilon_0 \varepsilon'}{E} \quad (3)$$

For this study, the target values are Young's modulus of 1 MPa and a dielectric constant of 5, which

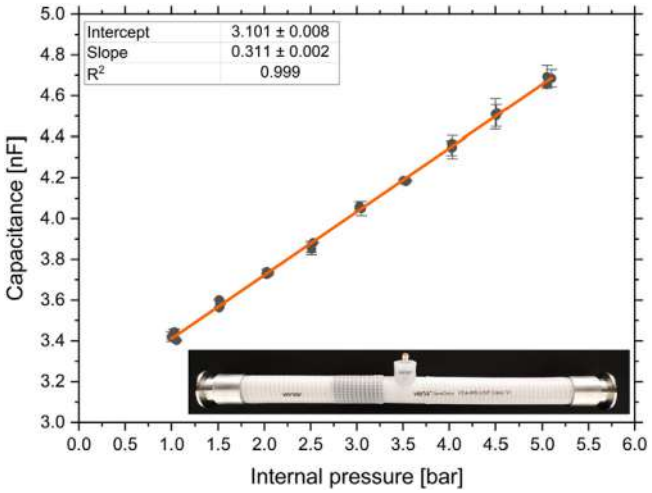

FIGURE 6 Response of the capacitive sensor prototype in the function of the pressure applied to the silicone rubber hose. The image corresponds to the sensor integrated into a Vena® Sil 650 V. [Color figure can be viewed at wileyonlinelibrary.com]

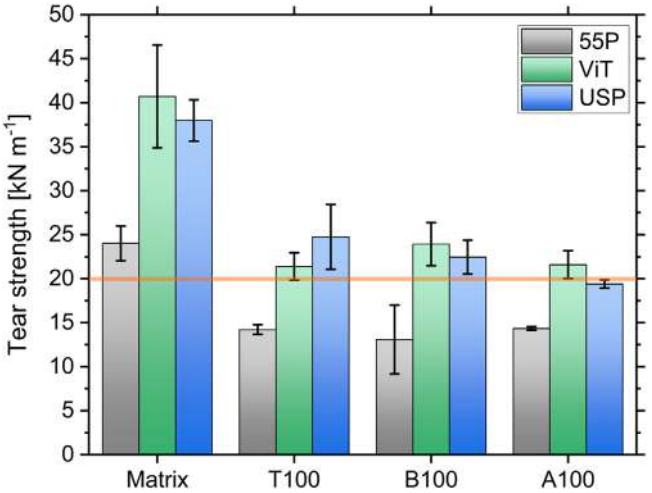

FIGURE 7 The tear strength of the dielectric composites with the 55P, ViT, and USP matrices. [Color figure can be viewed at wileyonlinelibrary.com]

corresponds to a FOM_{strain} of 3.1 F m N^{-1}. The results of the dielectric composites are shown in Figure 5.

The results indicate that incorporating TiO_2 or $BaTiO_3$ into LSR and USP matrices is insufficient to achieve the desired performance objectives. However, composites with ATO particles at 100 phr can significantly increase the dielectric constant to surpass Young's modulus increase, as can be seen in the USP matrix. All the composites prepared using the highly flexible ViT matrix meet the proposed objectives, including the matrix itself, which has a low Young's modulus. As expected, the addition of TiO_2 improves the electromechanical response compared to $BaTiO_3$, which requires further modifications to enhance the filler-polymer interaction.[60,61] The best results are obtained by adding ATO particles, which even at 50 phr, significantly increase FOM_{strain} compared to 100 phr of TiO_2 or $BaTiO_3$. When ATO particles are loaded at 100 phr, the large increase in dielectric constant and small increase in Young's modulus make this formulation the best-performing one in this study.

To provide insight into the industrial application of this type of dielectric silicone rubbers, the capacitive pressure sensors have been integrated inside a commercial silicone rubber hose to evaluate the capacity of the sensor to detect small deformations due to the pressure of the hose. The size of the sensor is 60 mm in width, 80 mm in height, and 250 μm thickness.

Figure 6 are presented the variation of the capacitance with the applied pressure in a benchmark system for maintenance and burst explosion analysis, as well as the image of the corresponding sensor's prototype.

The results showed that the sensor presents a linear and proportional response to the pressure, where the initial capacitance is $3.101 \pm 0.008\,nF^{-1}$, the sensitivity of the sensors is $311 \pm 2\,pF\,bar^{-1}$ and the corresponding pressure coefficient is $10,0193\,ppm\,bar^{-1}$.

3.5 | Mechanical integrity

Developing dielectric silicone rubber composites that maintain both mechanical integrity and processability is a major challenge. One crucial property indicative of mechanical robustness and durability is the tear strength, which is a demanding test for the material. Tear strength is essential for the proper manufacture and functioning of thin film devices that are subjected to mechanical stress and deformation. The recommended value for tear strength is typically 20 kN m^{-1} for flexible transducers.[13] Figure 7 presents a comparison of tear strength among the composites studied.

The LSR matrix selected for this study has a reference tear strength of 25 kN m^{-1}, but most commercial LSR formulations have lower tear strength. On the other hand, HCR grades typically have higher tear strength due to their high silica content and higher M_w. The measured tear strength of the 55P matrix meets the manufacturer's specifications, but the tear resistance is reduced below the threshold when 100 phr of dielectric fillers are added. Both HCR matrices show similar values, regardless of the cross-linking. Although the addition of dielectric fillers negatively affects the tear strength, the tear resistance of these composites is still significantly high enough to meet the required values.

4 | CONCLUSIONS

This paper explores the potential of using an HCR matrix to formulate dielectric composites with a high electromechanical response and fulfilling industrial requirements. The use of TiO_2/SnO_2-Sb as filler and a vinyl-terminated silicone gum has been proposed as an effective strategy to formulate these dielectric HCRs, increasing the dielectric constant while preserving Young's modulus. The comparison of these composites with TiO_2 and $BaTiO_3$ showed that ATO effectively increases the dielectric constant even at lower doses than the other fillers. Despite having a conductive layer, the ATO composites showed a high insulating behavior and the low $\tan\delta$ values indicate there are no significant dielectric relaxation processes. The ViT matrix has improved flexibility and retains Young's modulus even with a 100 phr of dielectric fillers loading The FOM_{strain} comparison confirmed that ATO at 50 phr with ViT matrix performs better than TiO_2 and $BaTiO_3$ at 100 phr. The best results are obtained with $\varepsilon' = 11.9 \pm 0.7$ and $E = 1.06 \pm 0.09$ when ATO is loaded at 100 phr. The HCR composites also exhibited better capability in retaining tear strength and mechanical integrity compared to LSR, making them more suitable for sensing applications and production processes.

Therefore, the developed ATO composites not only meet the properties needed for capacitive flexible sensors but are also formulated with commercially available products and manufactured with standard industrial processes and equipment, simplifying the industrial transfer of these technologies.

AUTHOR CONTRIBUTIONS

Joaquim Mª Rius-Bartra: Formal analysis (lead); investigation (equal); methodology (lead); writing – original draft (lead). **Norma Ferrer-Serrano:** Conceptualization (equal); funding acquisition (equal). **Núria Agulló:** Conceptualization (equal); investigation (equal); supervision (equal); writing – review and editing (lead). **Salvador Borrós:** Conceptualization (equal); funding acquisition (equal); supervision (equal); writing – review and editing (equal).

ACKNOWLEDGMENTS

We thank the Agència d'Ajuts Universitaris i de Recerca (AGAUR) as well as Departament de Recerca i Universitats of the Generalitat de Catalunya for the fellowship 2018 DI 062 to J. R. and for the SGR 2021 funding for GEMAT.

DATA AVAILABILITY STATEMENT

The data that support the findings of this study are available from the corresponding author upon reasonable request.

ORCID

Núria Agulló https://orcid.org/0000-0002-7712-0049
Salvador Borrós https://orcid.org/0000-0002-4003-0381

REFERENCES

[1] S.-T. Han, H. Peng, Q. Sun, S. Venkatesh, K.-S. Chung, S. C. Lau, Y. Zhou, V. A. L. Roy, *Adv. Mater.* **2017**, *29*, 1700375.
[2] Y. Yang, G. Chiesura, B. Plovie, T. Vervust, G. Luyckx, J. Degrieck, T. Sekitani, J. Vanfleteren, *ACS Sens.* **2018**, *3*, 1698.
[3] J. C. Costa, F. Spina, P. Lugoda, L. Garcia-Garcia, D. Roggen, N. Münzenrieder, *Technologies* **2019**, *7*, 35.
[4] Y. S. Rim, S. Bae, H. Chen, N. De Marco, Y. Yang, *Adv. Mater.* **2016**, *28*, 4415.
[5] F. Xu, X. Li, Y. Shi, L. Li, W. Wang, L. He, R. Liu, *Micromachines* **2018**, *9*, 580.
[6] R. B. Mishra, N. El-Atab, A. M. Hussain, M. M. Hussain, *Adv. Mater. Technol.* **2021**, *6*, 2001023.
[7] N. Wen, L. Zhang, D. Jiang, Z. Wu, B. Li, C. Sun, Z. Guo, *J. Mater. Chem. A* **2020**, *8*, 25499.
[8] B. Zazoum, K. M. Batoo, M. A. A. Khan, *Sensors* **2022**, *22*, 4653.
[9] R. Texidó, G. Nieva-Esteve, J. Gilabert-Porres, G. Reyes, S. Borrós, *Adv. Electron. Mater.* **2023**, *9*, 2200717.
[10] R. Li, Q. Zhou, Y. Bi, S. Cao, X. Xia, A. Yang, S. Li, X. Xiao, *Sens. Actuators, A* **2021**, *321*, 112425.
[11] Z. Ma, Y. Zhang, K. Zhang, H. Deng, Q. Fu, *Nano Mater. Sci.* **2022**. (In Press). https://doi.org/10.1016/j.nanoms.2021.11.002
[12] F. Carpi, I. Anderson, S. Bauer, G. Frediani, G. Gallone, M. Gei, C. Graaf, C. Jean-Mistral, W. Kaal, G. Kofod, M. Kollosche, R. Kornbluh, B. Lassen, M. Matysek, S. Michel, S. Nowak, B. O'Brien, Q. Pei, R. Pelrine, B. Rechenbach, S. Rosset, H. Shea, *Smart Mater. Struct.* **2015**, *24*, 105025.
[13] F. B. Madsen, A. E. Daugaard, S. Hvilsted, A. L. Skov, *Macromol. Rapid Commun.* **2016**, *37*, 378.
[14] A. L. Skov, L. Yu, *Adv. Eng. Mater.* **2018**, *20*, 1700762.
[15] Z.-M. Dang, Y.-J. Xia, J.-W. Zha, J.-K. Yuan, J. Bai, *Mater. Lett.* **2011**, *65*, 3430.
[16] H. Liu, L. Zhang, D. Yang, Y. Yu, L. Yao, M. Tian, *Soft Mater.* **2013**, *11*, 363.
[17] A. Bele, M. Cazacu, G. Stiubianu, S. Vlad, *RSC Adv.* **2014**, *4*, 58522.
[18] H. Zhao, L. Zhang, M.-H. Yang, Z.-M. Dang, J. Bai, *Appl. Phys. Lett.* **2015**, *106*, 092904.
[19] A. Bele, G. Stiubianu, C.-D. Varganici, M. Ignat, M. Cazacu, *J. Mater. Sci.* **2015**, *50*, 6822.
[20] L. Yu, A. L. Skov, *Int. J. Smart Nano Mater.* **2015**, *6*, 268.
[21] W. Schärtl, *Nanoscale* **2010**, *2*, 829.
[22] R. Ghosh Chaudhuri, S. Paria, *Chem. Rev.* **2012**, *112*, 2373.
[23] R. A. Ramli, W. A. Laftah, S. Hashim, *RSC Adv.* **2013**, *3*, 15543.
[24] S. Jiang, L. Jin, H. Hou, L. Zhang, *Polymer-Based Multifunctional Nanocomposites and Their Applications*, Elsevier, Amsterdam **2019**, p. 201.
[25] P. K. Kalambate, Dhanjai, Z. Huang, Y. Li, Y. Shen, M. Xie, Y. Huang, A. K. Srivastava, *TrAC, Trends Anal. Chem.* **2019**, *115*, 147.
[26] F. Lv, X. Feng, L. Yu, Y. Zhang, Z. Xu, *J. Mater. Res.* **2012**, *27*, 2489.

[27] Y. Wang, J. Qian, J. Xing, J. Xu, L. Liu, K. Ma, *J. Mater. Sci.* **2020**, *55*, 3871.
[28] Y. D. Wang, I. Djerdj, M. Antonietti, B. Smarsly, *Small* **2008**, *4*, 1656.
[29] J. Liu, X. Liu, Z. Zhai, G. Jin, Q. Jiang, Y. Zhao, C. Luo, L. Quan, *Sens. Actuators, B* **2015**, *220*, 1354.
[30] A. Sharma, A. Ahmed, A. Singh, S. K. Oruganti, A. Khosla, S. Arya, *J. Electrochem. Soc.* **2021**, *168*, 027505.
[31] H. Cochrane, C. S. Lin, *Rubber Chem. Technol.* **1993**, *66*, 48.
[32] Q. Xu, M. Pang, L. Zhu, Y. Zhang, S. Feng, *Mater. Des.* **2010**, *31*, 4083.
[33] S. C. Shit, P. Shah, *Natl. Acad. Sci. Lett.* **2013**, *36*, 355.
[34] A. Stricher, L. Picard, B. Gabrielle, E. Delebecq, F. Ganachaud, *Polym. Int.* **2016**, *65*, 713.
[35] E. A. Cherney, *IEEE Trans. Dielectr. Electr. Insul.* **2005**, *12*, 1108.
[36] Y. Gao, X. Liang, L. A. Dissado, S. J. Dodd, N. M. Chalashkanov, *IEEE Trans. Dielect. Electr. Insul.* **2016**, *23*, 3683.
[37] E. Delebecq, F. Ganachaud, *ACS Appl. Mater. Interfaces* **2012**, *4*, 3340.
[38] E. Delebecq, N. Hermeline, A. Flers, F. Ganachaud, *ACS Appl. Mater. Interfaces* **2012**, *4*, 3353.
[39] A. M. Stricher, R. G. Rinaldi, C. Barrès, F. Ganachaud, L. Chazeau, *RSC Adv.* **2015**, *5*, 53713.
[40] S. Park, K. Mondal, R. M. Treadway, V. Kumar, S. Ma, J. D. Holbery, M. D. Dickey, *ACS Appl. Mater. Interfaces* **2018**, *10*, 11261.
[41] ISO 23529:2010. General Procedures for Preparing and Conditioning Test Pieces for Physical Test Methods. Geneva: International Organization for Standardization. **2016**.
[42] ISO 34-1:2015. Rubber, Vulcanized or Thermoplastic—Determination of Tear Strength—Part 1: Trouser, Angle and Crescent Test Pieces. Geneva: International Organization for Standardization. **2015**.
[43] ISO 37:2017. Rubber, Vulcanized or Thermoplastic—Determination of Tensile Stress-Strain Properties. Geneva: International Organization for Standardization. **2017**.
[44] F. Müller, C. A. Ferreira, D. S. Azambuja, C. Alemán, E. Armelin, *J. Phys. Chem. B* **2014**, *118*, 1102.
[45] ASTM D150-98, Test Methods for AC Loss Characteristics and Permittivity (Dielectric Constant) of Solid Electrical Insulation, ASTM International. **1998**.
[46] M. Lisowski, A. Skopec, *IEEE Trans. Dielect. Electr. Insul.* **2009**, *16*, 24.
[47] Z. Xu, Y. Zhang, Y. Zhang, *Measurement* **2018**, *129*, 37.
[48] H.-G. Lee, J.-G. Kim, *Energies* **2020**, *13*, 2811.
[49] L. A. Fielding, J. K. Hillier, M. J. Burchell, S. P. Armes, *Chem. Commun.* **2015**, *51*, 16886.
[50] L. Liu, J. Qu, A. Gu, B. Wang, *J. Mater. Chem. A* **2020**, *8*, 18515.
[51] L. Ramajo, M. Reboredo, M. Castro, *Composit. A Appl. Sci. Manuf.* **2005**, *36*, 1267.
[52] C. V. Chanmal, J. P. Jog, *Express Polym. Lett.* **2008**, *2*, 294.
[53] M. Ben Omar, A. Matoussi. 2012 Annual Report Conference on Electrical Insulation and Dielectric Phenomena, IEEE, Montreal, QC, Canada, 2012, pp. 467–470.
[54] B. Benrabah, A. Bouaza, A. Kadari, M. A. Maaref, *Superlattices Microstruct.* **2011**, *50*, 591.
[55] V. K. Prateek, R. K. G. Thakur, *Chem. Rev.* **2016**, *116*, 4260.
[56] B. X. Du, Z. L. Li, Z. R. Yang, *IEEE Trans. Dielect. Electr. Insul.* **2016**, *23*, 3108.
[57] Z.-H. Shen, J.-J. Wang, X. Zhang, Y. Lin, C.-W. Nan, L.-Q. Chen, Y. Shen, *Appl. Phys. Lett.* **2017**, *111*, 092901.
[58] K. Ghosh, J. Guo, O. Lopez-Pamies, *Int. J. Non-Linear Mech.* **2019**, *116*, 155.
[59] N. Della Schiava, K. Thetpraphi, M.-Q. Le, P. Lermusiaux, A. Millon, J.-F. Capsal, P.-J. Cottinet, *Polymer* **2018**, *10*, 263.
[60] L. Jiang, A. Betts, D. Kennedy, S. Jerrams, *Mater. Des.* **2015**, *85*, 733.
[61] D. Yang, X. Kong, Y. Ni, Y. Xu, S. Huang, G. Shang, H. Xue, W. Guo, L. Zhang, *ACS Omega* **2018**, *3*, 14087.

SUPPORTING INFORMATION

Additional supporting information can be found online in the Supporting Information section at the end of this article.

How to cite this article: J. M. Rius-Bartra, N. Ferrer-Serrano, N. Agulló, S. Borrós, *J. Appl. Polym. Sci.* **2023**, *140*(37), e54405. https://doi.org/10.1002/app.54405